Robust Design of Countercurrent Adsorption Separation Processes: 5. Nonconstant Selectivity

Cristiano Migliorini and Marco Mazzotti
ETH Zürich, Institut für Verfahrenstechnik, Sonneggstrasse 3, CH-8092 Zürich, Switzerland

Massimo Morbidelli
ETH Zürich, Laboratorium für Technische Chemie, Universitätstrasse 6, CH-8092 Zürich, Switzerland

Operating conditions for the separation of a binary mixture using a nonadsorbable eluent through simulated moving-bed technology were designed. The results obtained using equilibrium theory for adsorption described by Langmuir models lead to the definition of explicit constraints on the operating parameters to operate the unit in the desired regime of separation. A more general approach was able to produce the same result for a larger class of isotherms. The physical and mathematical conditions defining this larger class of isotherms are discussed, as well as the algorithms necessary to calculate the region of complete separation. Applications to the bi-Langmuir isotherm and the ideal adsorbed solution model, which are more flexible than the Langmuir model and can describe systems where selectivity changes with composition, are discussed. A shortcut method to get an explicit, though approximate, solution is proposed and its accuracy is discussed.

Introduction

During the last few years, continuous chromatography, through the simulated moving-bed (SMB) technology, has been applied more and more extensively to the separation of valuable compounds such as enantiomeric mixtures. The development of continuous chromatographic separations for industrial processes requires a thorough study of the design criteria and a better understanding of the nonlinear behavior exhibited under overload conditions (Mazzotti et al., 1997a). In previous works the optimal operating conditions for a true countercurrent (TCC) adsorptive separation unit have been found through the application of Equilibrium Theory, that is, neglecting axial dispersion and mass-transfer resistance (Storti et al., 1993; Mazzotti et al., 1994, 1996b, 1997b; Gentilini et al., 1998; Chiang, 1998a,b). In spite of the mathematical complexity of the problem, the solution can be given through simple relationships that constrain the dimensionless parameters m_j, defined as the ratio of fluid to solid flow rates in each section of the unit. This leads to the partitioning of the (m_2, m_3) plane, that is, the operating parameter plane spanned by the flow-rate ratios in the two key sections of the unit, into several regions corresponding to all possible separation regimes: both raffinate and extract are pure; either one of them, but not both, is pure; neither is pure. This approach, which is often referred to as the ''Triangle Theory'' for the characteristic shape of the complete separation region (that is, where both raffinate and extract are pure), has been validated by comparison with experimental data (Storti et al., 1993; Mazzotti et al., 1996a; Pedeferri et al., 1999) and applied to investigate various separations (Mazzotti et al., 1997b; Francotte et al., 1998; Migliorini et al., 1998, 1999a). The Triangle Theory provides a clear picture of the different separation regions in the operating parameter space, which is somehow universal, since it depends only on the thermodynamics of adsorption, on the size of the unit or on productivity and flow rates, and provides a reliable first approximation for the optimal operating conditions, which are then refined by accounting for dispersion mechanisms (that is, transport resistance and axial dispersion) through classic detailed models to be solved numerically (Migliorini et al., 1999a).

Correspondence concerning this article should be addressed to M. Morbidelli.
The previous parts of this series were presented by Storti et al., 1993, and by Mazzotti et al., 1994, 1996b, 1997b.

Unfortunately, at present, Triangle Theory is available only for stoichiometric and nonstoichiometric Langmuir isotherms. In this case, in fact, the relevant steady-state partial differential equations can be solved explicitly through an appropriate orthogonalization technique, that is, the ω-transformation (Rhee et al., 1970) or the equivalent h-transformation (Helfferich and Klein, 1970). However, this technique is not general and it has been developed only for the isotherms just mentioned, which are suitable to describe competitive adsorption equilibria only in the case of constant selectivity. In many cases of practical interest, this limitation is too strict since the complex adsorbate–adsorbate or adsorbate–adsorbent interactions lead to selectivities that vary with composition. Examples are several chiral separations, where the enantiomers to be separated interact with both chiral and achiral sites of the stationary phase, and a bi-Langmuir isotherm can be used to describe the adsorption equilibrium data (Jacobson et al., 1990; Fornstedt et al., 1997; Gentilini et al., 1998); in other cases, more complex interactions require more complex models (Seidel-Morgenstern and Guiochon, 1993; Pedeferri et al., 1999).

The aim of this work is to provide a procedure in the frame of Equilibrium Theory to calculate the boundaries of the complete separation region in the operating parameter plane (m_2, m_3) and the critical values for m_1 and m_4 in the case of binary mixtures described by a general adsorption isotherm. This can be done when a set of physical and mathematical conditions are satisfied and allows the case of selectivity changing with composition to be included. The price to be paid for such an extension is that, in some cases (but not always), the procedure developed requires the numerical integration of ordinary differential equations; among the systems for which this approach is valid are some systems described by the bi-Langmuir isotherm, which is typically used to describe adsorption equilibria of enantiomers, and some systems whose equilibria can be described through the Ideal Adsorption Solution Theory (IAS) (Radke and Prausnitz, 1972; Antia and Horváth, 1991; Seidel–Morgenstern and Guiochon, 1993). Examples of application are discussed.

Design Problem

The details of the principles of SMB units (see Figure 1) can be found in many previous works (cf. Ruthven and Ching, 1989 and the previous parts of this series). The key idea is to simulate in the SMB the solid-phase motion of the corresponding TCC unit by periodically switching the inlet and outlet ports of the unit in the same direction of the fluid flow (with period t^*). The following set of relationships establishes the operating parameters of TCC and SMB units that allow the same separation performances to be achieved (see the Notation section for the meaning of the symbols):

$$Q_j^{\mathrm{SMB}} = Q_j^{\mathrm{TCC}} + Q_S \frac{\epsilon_b}{1-\epsilon_b} \tag{1}$$

$$Q_S = (1-\epsilon_b)\frac{V}{t^*}. \tag{2}$$

Based on these equations, the cyclic steady state of an SMB (simulated moving bed) unit can be studied by considering the steady state of the equivalent four-section TCC (true countercurrent) unit illustrated in Figure 2 (Ruthven and Ching, 1989; Migliorini et al., 1999b). In the frame of the Equilibrium Theory and with reference to Figure 3, the dimensionless mass-balance equation for the ith species in the jth section of the TCC unit is given as follows:

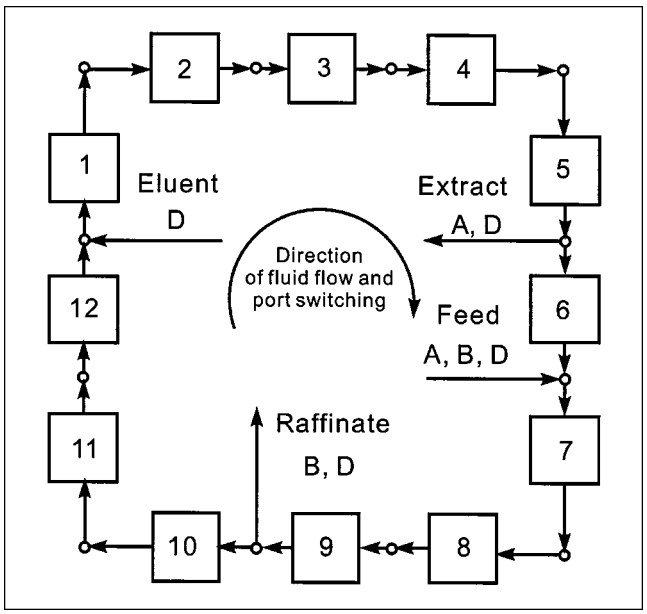

Figure 1. Simulated moving-bed unit for continuous chromatographic separations, with port configuration 5-1-3-3.

$$\frac{\partial}{\partial \tau}\left[\epsilon^* c_i^j + (1-\epsilon^*) n_i^j\right] + (1-\epsilon_p)\frac{\partial}{\partial x}\left(m_j c_i^j - n_i^j\right) = 0. \tag{3}$$

In the previous equation, axial dispersion is neglected and local equilibrium is assumed according to the relationship:

$$n_i^j = n_i^j(c). \tag{4}$$

Notice that the net flux of species i in section j,

$$f_i^j = Q_S(1-\epsilon_p)\left(m_j c_i^j - n_i^j\right), \tag{5}$$

depends on the dimensionless flow-rate ratio parameter:

$$m_j = \frac{Q_j^{\mathrm{TCC}} - \epsilon_p Q_S}{Q_S(1-\epsilon_p)}. \tag{6}$$

For a binary mixture in a nonadsorbable carrier, we will define A and B as the more- and less-retained component, respectively. The objective is to determine the set of operating conditions that allow complete separation to be achieved, that is, to collect the strong component A pure in the extract and the weak component B pure in the raffinate. To this aim and in order to collect pure product streams and to properly regenerate the eluent in section 4 and the stationary phase in section 1, the following sign conditions for the net fluxes (Eq.

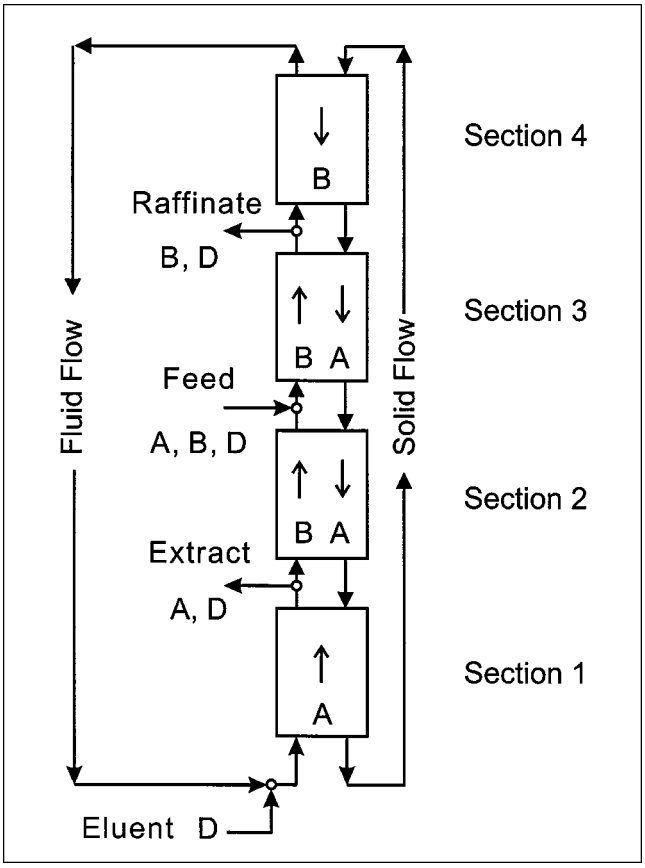

Figure 2. Four-section true countercurrent unit for continuous chromatographic separations.

5) must be fulfilled (see Figure 2):

$$\text{Section 1: } f_A^1 \geq 0; \quad f_B^1 \geq 0 \tag{7}$$

$$\text{Section 2: } f_A^2 \leq 0; \quad f_B^2 \geq 0 \tag{8}$$

$$\text{Section 3: } f_A^3 \leq 0; \quad f_B^3 \geq 0 \tag{9}$$

$$\text{Section 4: } f_A^4 \leq 0; \quad f_B^4 \leq 0. \tag{10}$$

By using Eq. 5, these inequalities can be expressed as constraints on the m_j parameters:

$$\text{Section 1: } m_1 \geq \frac{n_A^1}{c_A^1}; \quad m_1 \geq \frac{n_B^1}{c_B^1} \tag{11}$$

$$\text{Section 2: } \frac{n_B^2}{c_B^2} \leq m_2 \leq \frac{n_A^2}{c_A^2} \tag{12}$$

$$\text{Section 3: } \frac{n_B^3}{c_B^3} \leq m_3 \leq \frac{n_A^3}{c_A^3} \tag{13}$$

$$\text{Section 4: } m_4 \leq \frac{n_A^4}{c_A^4}; \quad m_4 \leq \frac{n_B^4}{c_B^4}. \tag{14}$$

It is worth noting that since, in the frame of Equilibrium Theory at steady state, each section of a countercurrent unit

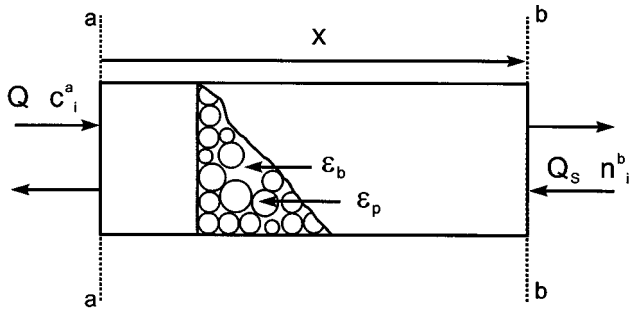

Figure 3. Countercurrent column.

The fluid feed enters from the boundary *aa*, the solid feed enters from the boundary *bb*.

reaches a constant composition profile (or constant state), the superscripts in the preceding equations indicate the constant state prevailing in each section. In a sense that we will clarify later, such steady-state profiles are a function of the operating parameters, m_j, so that the constraints expressed in Eqs. 11–14 are at this stage implicit.

By imposing these constraints one can define the region of complete separation in the space spanned by the four coordinates m_1, m_2, m_3, and m_4. Except for the case of linear adsorption equilibrium, which is trivial, this has been done using the orthogonalization technique mentioned earlier, which is strictly confined to the use of Langmuir-type isotherms, including the nonstoichiometric, stoichiometric, and the modified Langmuir isotherms. All these isotherms imply constant selectivity, with the only exception of the modified Langmuir isotherm, which, however, can account only for small selectivity variations. In this article we present a new approach for making the constraints in Eqs. 11–14 explicit, which is based on the direct application of the method of characteristics rather than on the use of orthogonalization techniques, which are actually just a special way of applying the method of characteristics itself. This approach can be applied to a much larger class of isotherms, provided that a set of physical and mathematical conditions are fulfilled. In particular, to this class belong many systems among those described by the bi-Langmuir and the multicomponent IAS model that account for large variations of selectivity, with composition often encountered in applications. In the following we derive the new procedure and illustrate the corresponding algorithms. The reader not interested in the mathematical details can go directly to the fourth section, where the influence of nonconstant selectivity in the adsorption equilibria on the separation performance is discussed.

Design of the Operating Conditions

In this section the procedure to determine the complete separation region in the operating parameter space for a general adsorption isotherm is described; this approach is based on the theory of hyperbolic, reducible, homogeneous, first-order partial differential equations (Rhee et al., 1989). We proceed through the following steps:

1. First, we show how the operating parameter m of a single countercurrent bed should be selected in order to achieve a desired steady state (in the following subsection).

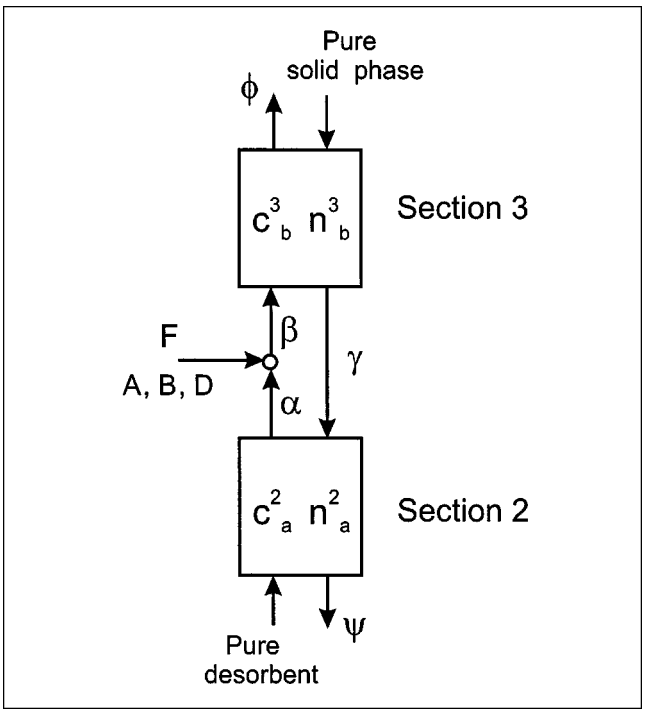

Figure 4. Two-section countercurrent unit.

Pure desorbent and regenerated solid enter sections 2 and 3, respectively.

2. The two-section TCC unit illustrated in Figure 4, which is constituted of the coupling of two countercurrent sections, is considered. Using the results of the previous point, we determine the steady-states corresponding to the m_2 and m_3 values that satisfy Eqs. 12 and 13, and therefore lead to complete separation (see the subsection titled ''Two-Section TCC Unit'').

3. The equations and algorithms needed to calculate the complete separation region in the (m_2, m_3) plane are described in the subsection on that subject.

4. The results obtained for a two-section TCC unit are extended to a four-section TCC unit in the subsection titled ''Four-Section TCC Unit'' by properly selecting the values of the m parameters in the regenerating sections, that is, m_1 and m_4, so as to fulfill the constraints given by Eqs. 11 and 14.

It should be noted that the development of this approach requires that the adsorption isotherms satisfy the following conditions:

- The isotherms are purely competitive, as

$$\frac{\partial n_i}{\partial c_i} > 0 \qquad i = A,\ B \tag{15}$$

$$\frac{\partial n_i}{\partial c_j} < 0 \qquad i \neq j. \tag{16}$$

- The variation of c_i has a stronger influence on the adsorption of component i itself than on the adsorption of the other components, that is,

$$\frac{\partial n_i}{\partial c_i} > \left| \frac{\partial n_j}{\partial c_i} \right|. \tag{17}$$

Note that Eqs. 15 and 17 imply that there exists a one-to-one mapping between fluid and adsorbed phase compositions, hence the equations

$$n_A = n_A(c_A, c_B) \tag{18}$$

$$n_B = n_B(c_A, c_B) \tag{19}$$

are invertible everywhere in the hodographic plane (c_A, c_B). This can be readily seen by inspection of the Jacobian matrix of the mapping equations (Eqs. 18 and 19) in the case where Eqs. 15 and 17 are satisfied. It is worth noticing that, as is typical in most fine chemical applications, we are assuming that the components to be separated are diluted in an inert solvent, which plays the role of nonadsorbable desorbent in the separation.

- The pure-component isotherms are favorable for any given value of the other component:

$$\left(\frac{\partial^2 n_i}{\partial c_i^2} \right)_{c_j} < 0. \tag{20}$$

By inspection of these conditions it appears that they are typical of favorable, competitive isotherms, which are by far the most common in applications.

Single countercurrent section

Let us consider the countercurrent adsorption column illustrated in Figure 3. For the sake of simplicity in this subsection, we drop the index j in all variables and parameters used in Eqs. 3 to 6. Equation 3 must be solved together with the following boundary and initial conditions, which are assumed to be constant:

$$c_i(0, \tau) = c_i^a \qquad \tau > 0 \tag{21}$$

$$n_i(1, \tau) = n_i^b \qquad \tau > 0 \tag{22}$$

$$c_i(x, 0) = c_i^i \qquad 0 < x < 1. \tag{23}$$

These define a so-called Riemann problem.

With reference to Figure 3, there are a fluid and a solid inlet state, namely states a and b corresponding to points (c_A^a, c_B^a) and (c_A^b, c_B^b), respectively; here (c_A^b, c_B^b) represents the fluid-phase composition in thermodynamic equilibrium with the adsorbed phase inlet composition (n_A^b, n_B^b), according to Eqs. 18 and 19. It can be proved that a constant steady-state solution of the Riemann problem, homogeneous in space, is achieved, which depends only on the boundary conditions and the flow rate ratio m. This can be determined by analyzing the composition path $a \rightarrow M \rightarrow b$ in the hodograph plane, where M is an intermediate state characterized by the composition (c_A^M, c_B^M). The procedure to build the composition

Table 1. Analysis of the Steady Behavior of a Countercurrent Column

Range	m Range	Constant Steady-State
Lower range	$-\epsilon_p/(1-\epsilon_p) \le m \le m_1^*$	Adsorbed Phase State, b
1-Transition range	$m_1^* < m < m_{1,*}$	State along characteristic Γ_1
Intermediate range	$m_{1,*} \le m \le m_2^*$	Intermediate state, M
2-Transition range	$m_2^* < m < m_{2,*}$	State along characteristic Γ_2
Upper range	$m_{2,*} \le m < \infty$	Fluid-phase state, a

path in the hodograph plane and to determine the intermediate state M is summarized in Appendix A. In general, the path $a \rightarrow M$ belongs to either a Γ_2 or a Σ_2 transition originating from point a, whereas the path $M \rightarrow b$ belongs to either a Γ_1 or a Σ_1 transition originating from point b. As discussed in Appendix A, the Γs are continuous transitions, referred to also as simple waves, whereas the Σs are discontinuous transitions, called shock waves.

The final result is that the constant steady state prevailing in the countercurrent section is selected through the value of the flow-rate ratio m according to the rules reported in Table 1. It turns out that a unique steady state corresponds to each of the lower, upper, and intermediate ranges, while a continuum of steady states is associated to each transition range. When the kth transition is a shock wave, then $m_{k,*} = m_k^*$ and the k-transition range degenerates into a single value. The nature of each transition is uniquely determined by the relative position of states a and b in the hodograph plane; hence, it is rather easy to determine *a priori* the expressions for the bounds in the inequalities of Table 1.

If both transitions are simple waves, that is, a Γ_1 and a Γ_2 in the hodograph plane, then the bounds are given by the following relationships:

$$m_1^* = \beta_1|_b, \tag{24}$$

$$m_{1,*} = \beta_1|_M, \tag{25}$$

$$m_2^* = \beta_2|_M, \tag{26}$$

$$m_{2,*} = \beta_2|_a, \tag{27}$$

where the subscript indicates the point in the hodograph plane where the parameter β, given by Eq. A1 of Appendix A, must be evaluated. If both transitions are shock waves, that is, a Σ_1 and a Σ_2 in the hodograph plane, then there are only two bounds that are given by the following relationships:

$$m_1^* = m_{1,*} = \tilde{\beta}_1|_{M \rightarrow b} \tag{28}$$

$$m_2^* = m_{2,*} = \tilde{\beta}_2|_{a \rightarrow M}. \tag{29}$$

The cases where one transition is a simple wave and the other is a shock wave can be simply derived by properly combining Eqs. 24 to 29.

In this brief summary of the results of Equilibrium Theory we have assumed that the transitions connecting two points in the hodograph plane are always either shocks or simple waves, combined situations as combined waves (such as semishocks) being excluded. The stability conditions that guarantee these assumptions for transitions in the two-section TCC unit are better clarified in Appendix B. It is worth noting that these assumptions are always fulfilled by the Langmuir and the modified Langmuir isotherm. However, this is not necessarily the case for all types of isotherms, and there may be instances where strong differences in terms of sequence of transitions may arise. The procedure to draw the region of separation presented below can be applied only if the transitions connecting two points in the hodographic plane are shocks or simple waves, that is, no combined waves are present. In other words, the transitions pertaining to section 2 of the separation unit, corresponding to elution steps, must be simple waves, whereas those pertaining to section 3, corresponding to adsorption steps, must be shocks. These prerequisites for the application of the method are stated in mathematical terms in Appendix B, where an algorithm to check the fulfillment of these conditions is presented.

Two-section TCC unit

Let us consider the two-section TCC unit shown in Figure 4, where we assume that both the desorbent and the solid phase fed to the unit contain neither component A nor component B, that is, they have been somehow fully regenerated. Accordingly, both these states are represented in the hodograph plane in Figure 5 by the origin and therefore, as shown in Appendix A, the intermediate state M for sections 2 and 3 lies on the axes c_A and c_B, respectively, or $M = M_2 = (c_A^2, 0)$ in section 2 and $M = M_3 = (0, c_B^3)$ in section 3. In other words, state M_2 is pure A and M_3 is pure B.

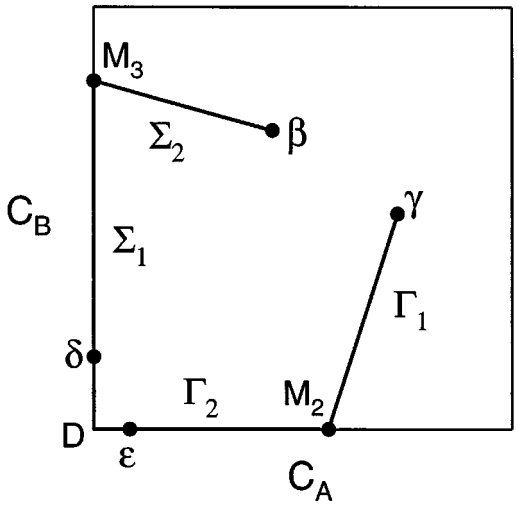

Figure 5. Transition paths in the (c_A, c_B) plane for section 3 ($\beta \rightarrow M_3 \rightarrow D$) and section 2 ($D \rightarrow M_2 \rightarrow \gamma$) in two-section TCC unit.

In a four-section TCC unit the point D is replaced with δ and ϵ, which represents the solid-state entering section 3 and the fluid state entering section 2, respectively.

Let us now determine separately for each of the two sections of the unit the kind of steady states that guarantee complete separation, based on the conditions for complete separation in terms of single species fluxes, that is, Eqs. 7 to 10 and on the Equilibrium Theory analysis of the single countercurrent section summarized earlier. At this stage, the feed stream and streams $\boldsymbol{\beta}$, entering section 3 as a fluid, and $\boldsymbol{\gamma}$, representing the solid leaving section 3, are considered not to be coupled; they all fulfill the requirement of containing both components A and B. The result can be summarized in the following theorem, whose proof is reported in Appendix C:

Theorem. Necessary and sufficient conditions for complete separation in the two-section TCC unit in Figure 4 are that the two sections operated at the intermediate states $M_2 = (c_A^2, 0)$ and $M_3 = (0, c_B^3)$.

Complete separation region

Using the preceding theorem [the requirement of having simple waves in section 2 and shock waves in section 3 (see Appendix B)], Table 1, and Eqs. 24 to 29, the conditions to achieve complete separation in a two-section TCC unit can be cast as follows:

$$\beta_1|_{M_2} = m_{2,\min} \le m_2 \le m_{2,\max} = \beta_2|_{M_2} \tag{30}$$

$$\tilde{\beta}_1|_{M_3 \to D} = m_{3,\min} \le m_3 \le m_{3,\max} = \tilde{\beta}_2|_{\beta \to M_3}. \tag{31}$$

The boundaries of the complete separation region are defined by the relationships obtained when m_2 and m_3 attain the upper and lower bounds in the previous inequalities. Using the results of Appendix A, these can be written as follows:

$$m_{2,\min} = \left.\frac{\partial n_B}{\partial c_B}\right|_{M_2} \tag{32}$$

$$m_{2,\max} = \left.\frac{\partial n_A}{\partial c_A}\right|_{M_2} \tag{33}$$

$$m_{3,\min} = \frac{n_B^3}{c_B^3} \tag{34}$$

$$m_{3,\max} = \frac{n_B^\beta - n_B^3}{c_B^\beta - c_B^3} = \frac{n_A^\beta}{c_A^\beta}, \tag{35}$$

where the superscripts 3 and β refer to the states M_3 and $\boldsymbol{\beta}$, respectively.

Before analyzing these equations to gain more insight about the boundary of the complete separation region, it is worth noting that states $\boldsymbol{\beta}$ and $\boldsymbol{\gamma}$ in Figures 4 and 5 are, in general, different, though coupled through mass balances at the bottom of section 3. However, when $m_3 = m_{3,\max}$, then $\boldsymbol{\beta} = \boldsymbol{\gamma}$, as illustrated in Figure 6. In this case, in fact, the mass balances at the bottom of section 3 are

$$\left(m_3 + \frac{\epsilon_p}{1-\epsilon_p}\right) c_A^\beta - n_A^\gamma - \frac{\epsilon_p}{1-\epsilon_p} c_A^\gamma = 0 \tag{36}$$

$$\left(m_3 + \frac{\epsilon_p}{1-\epsilon_p}\right) c_B^\beta - n_B^\gamma - \frac{\epsilon_p}{1-\epsilon_p} c_B^\gamma = m_3 c_B^3 - n_B^3, \tag{37}$$

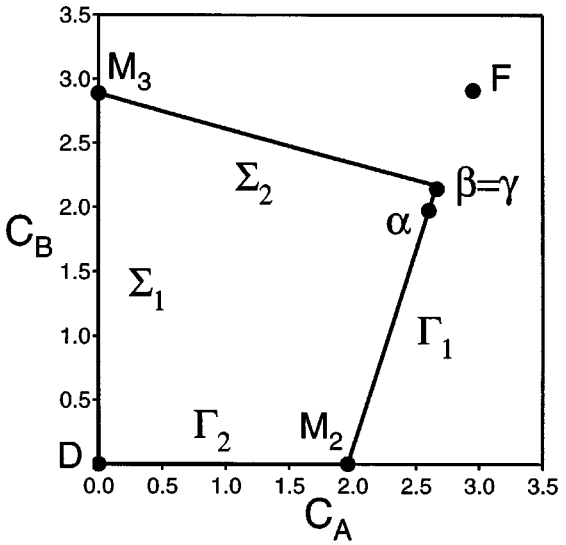

Figure 6. Transition paths in the (c_A, c_B) plane in a two-section TCC unit for the optimal operating point w at a feed concentration of $c_A^F = c_B^F = 2.9$ g/L.

The bi-Langmuir isotherm parameters are: $\gamma_A = 3.728$, $\delta_A = 0.3$, $a_A = 0.0466$ g/L, $b_A = 3$ g/L, $\gamma_B = 2.688$, $\delta_B = 0.1$, $a_B = 0.0336$ g/L, $b_B = 1$ g/L.

where the superscript γ refers to the state $\boldsymbol{\gamma}$. Combining these with Eq. 35 proves that indeed $c_i^\beta = c_i^\gamma$ and $n_i^\beta = n_i^\gamma$, for $i = A, B$. It is worth observing that in this case the net fluxes of components A and B through section 3 given by Eq. 5 can be recast using Eq. 35 in terms of the state $\boldsymbol{\beta}$:

$$f_i^3 = Q_S(1-\epsilon_p)\left(m_3 c_i^\beta - n_i^\beta\right) \qquad (i = A, B). \tag{38}$$

With reference to Figure 6, it can be seen that since points $\boldsymbol{\beta}$ and $\boldsymbol{\gamma}$ coincide, then the two paths corresponding to sections 2 and 3—$\boldsymbol{\beta} \to M_3 \to D$ and $D \to M_2 \to \boldsymbol{\gamma}$—constitute a closed loop. Moreover, note that the feed state is different from $\boldsymbol{\beta} = \boldsymbol{\gamma}$ and that states $\boldsymbol{\alpha}$, $\boldsymbol{\beta}$, and F are on a straight line due to the constraint provided by the material balance at the feed node.

Let us now analyze each portion of the boundary in detail. For this, we use the same notation adopted in previous articles (see Figure 7, which is calculated for a system described by a bi-Langmuir isotherm, as discussed in detail in the subsection titled ''Bi-Langmuir Isotherm''). In all four following cases the overall mass balances for components A and B under the assumption of complete separation must be fulfilled:

$$(m_3 - m_2) c_A^F = n_A^2 - m_2 c_A^2 \tag{39}$$

$$(m_3 - m_2) c_B^F = m_3 c_B^3 - n_B^3. \tag{40}$$

Curve ab: $m_3 = m_{3,\min}$, Eq. 34. In this case the r.h.s. of Eq. 40 is zero, hence $m_3 = m_2$. This yields the portion *ab* of the diagonal; the coordinates of points *a* and *b* are the Henry's constants of components A and B, respectively, that is, the slope of the single-component isotherms at zero concentration.

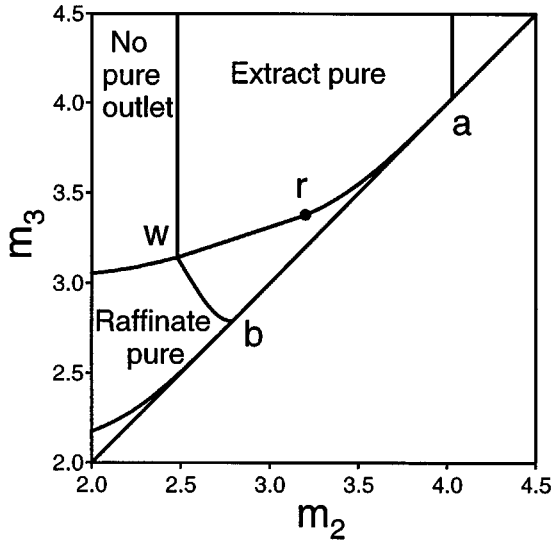

Figure 7. Regions of separation in the (m_2, m_3) plane for the bi-Langmuir isotherm: the parameters and the composition of the feed mixture are the same as in Figure 6.

Both regions of separation intersect the diagonal of the operating plane at points *a* and *b* of coordinates (H_A, H_A) and (H_B, H_B).

Curve wb: $m_2 = m_{2,\min}$, Eq. 32. Let us take c_A^2 as a running parameter along this part of the boundary, starting from point *b* on the diagonal; here the fluid flow rate is zero and c_A^2 is also necessarily zero. With the chosen value of c_A^2, m_2 is obtained from Eq. 32. Substituting into Eq. 39 yields the corresponding m_3 value. The endpoint *w* of the curve is obtained as the intercept with *wr* (see below).

Curve ra: $m_2 = m_{2,\max}$, Eq. 33. Equation 33 is now applied to calculate m_2, again using c_A^2 as a running parameter (initial value $c_A^2 = 0$) and Eq. 39 to obtain m_3. It is worth noting that this portion of the boundary depends only on the pure-component isotherm of component *A*. The endpoint *r* is the intercept with curve *wr*. It is worth noting that due to the use of Eq. 39, curves *wb* and *ra* depend only on c_A^F rather than on the whole composition of the feed (Gentilini et al., 1998).

Curve wr: $m_3 = m_{3,\max}$, Eq. 35. As just discussed, in this case $\boldsymbol{\beta} = \boldsymbol{\gamma}$, hence Figure 6 applies and the determination of this part of the boundary is more difficult than in the previous cases. Besides Eqs. 35 and the overall balances for *A* and *B*, that is, Eqs. 39 and 40, another constraint is that the states $\boldsymbol{\beta}$ and M_2 must belong to the same Γ_1, that is, they must be obtained one from the other through integration along Γ_1 according to the procedure described in Appendix A. These five constraints allow the five unknowns m_2, m_3, c_A^2, c_A^β, and c_B^β to be determined once a value of the running parameter along *wr* c_B^3 is given. An upper bound for c_B^3 is provided by the value obtained from Eqs. 35, when $c_i^\beta = c_i^F$. It is worth noticing that in the optimal point *w*, Eqs. 32 and 35 are fulfilled together with the overall mass balances for *A* and *B* under complete separation. This means that in *w* the m_2 and m_3 parameters are, respectively, the smallest and largest achievable to realize the constant states required by the theorem introduced at the end of the previous subsection. The solution of the four algebraic equations plus the ordinary differential equation, though in principle always feasible, may in practice be rather cumbersome for complex isotherms. This is particularly true because the conditions for the applicability of the method must be controlled during the determination of this portion of the boundary of the complete separation region, as discussed in Appendix B.

Four-section TCC unit

The four-section TCC unit shown in Figure 2 can be regarded as the two-section unit where two more sections have been added. Section 1 at the bottom is used to regenerate the solid, and section 4 at the top is used to regenerate the desorbent. In this way, we can obtain a complete process including the regeneration steps. This poses two problems: the first is how to design the operating parameters m_1 and m_4 in sections 1 and 4, respectively, so as to make sure that the regeneration processes are properly performed; this is of the greatest importance, since the expected separation regimes determined by the position of the operating point in the (m_2, m_3) plane are attained only if a complete regeneration is achieved in sections 1 and 4 (Storti et al., 1993; Migliorini et al., 1998, 1999a). The second is whether and how the analysis developed for sections 2 and 3 with reference to the two-section TCC unit can be extended.

First, let us analyze the regenerating sections. The same principles mentioned earlier can be applied to this case in an even more simple way, because only single-component adsorption is involved, provided that complete separation is achieved in sections 2 and 3. Since both pure isotherms are assumed to be favorable as to Eq. 20, one can easily prove that the single transition occurring from the state of pure *B* to the pure solid state in section 4 is a Σ shock, that is, corresponding to adsorption of *B* on a regenerated solid phase, while, on the other hand, the transition between the pure fluid state and the state of pure *A* in section 1 is a Γ simple wave, that is, corresponding to elution of an adsorbed species.

In section 4 the prevailing steady state must be the solid state, that is, *B* entering the column must be completely adsorbed and carried downwards to the raffinate node. The corresponding constraint on the flow rate ratio is

$$\frac{\epsilon_p}{\epsilon_p - 1} \le m_4 \le m_{4,\max} = \frac{n_B\left(c_B^R\right)}{c_B^R}, \tag{41}$$

where $m_{4,\max}$ is the value that allows the shock transition corresponding to the adsorption front of *B* standing in section 4 (Rhee et al., 1986), whereas m_4 attains the l.h.s. of the inequality when $Q_4 = 0$ and the separation unit is operated with three sections only (Mazzotti et al., 1996a). The raffinate concentration c_B^R can be obtained from the overall mass balance of *B* in a four-section TCC unit under the assumption of complete separation:

$$(m_3 - m_2)c_B^F = (m_3 - m_4)c_B^R. \tag{42}$$

Therefore, the value of $m_{4,\mathrm{cr}}$ depends on the values of m_2, m_3, and c_B^F. Due to Eq. 20, Eq. 41 indicates that $m_{4,\max}$ decreases when c_B^F and c_B^R increase and that its maximum

value is the Henry constant of species B, that is, the infinite dilution slope of its isotherm, H_B.

In section 1 the prevailing steady state must be the fluid state, so that component A is completely desorbed by the fluid flow and carried upwards to the extract node. This condition is guaranteed by the condition

$$m_1 \geq m_{1,\min} = \left.\frac{dn_A(c_A)}{dc_A}\right|_{c_A=0} = H_A. \qquad (43)$$

When the two constraints (Eqs. 41 and 43) are fulfilled, it is guaranteed that the fluid stream entering section 2 contains some component A but no B, while, on the other hand, the solid stream fed to section 3 has some component B adsorbed, but no A. Therefore with reference to Figure 5, these states correspond in the hodograph plane to points $\boldsymbol{\epsilon}$ and $\boldsymbol{\delta}$, respectively. The second issue about four-section TCC units is exactly whether this new situation can affect the values of m_2 and m_3 leading to complete separation that were computed earlier for the two-section TCC unit. The answer is negative for three reasons. First, in the four-section unit also, sections 2 and 3 must attain the intermediate states $\boldsymbol{M}_2$ and $\boldsymbol{M}_3$ to achieve complete separation, as proved in Appendix C. Second, among the four constraints defining the boundaries of the complete separation region, that is, Eqs. 32 to 35, three depend on states $\boldsymbol{\beta}$, $\boldsymbol{M}_2$ and $\boldsymbol{M}_3$, whereas only $m_{3,\min}$ is given by a different relationship involving the state $\boldsymbol{\delta}$, namely Eq. C5 in Appendix C. Since $m_3 = m_{3,\min}$ leads to $f_B^3 = 0$ (see Appendix C), in a four-section TCC unit this condition also is mapped onto the diagonal of the (m_2, m_3) plane. Finally, under complete separation conditions for both the two- and the four-section units with the same feed composition and the same choice of m_2 and m_3 the overall material balances (Eqs. 39 and 40) must be fulfilled; these obviously yield the same $\boldsymbol{M}_2$ and $\boldsymbol{M}_3$ states, which, combined with the same feed state, yield the same state $\boldsymbol{\beta}$, and hence, the same conditions for complete separation (Eqs. 32, 33 and 35) as required by the statement.

Thus, it can be concluded that the complete separation region obtained in the previous subsection for the two-section TCC unit also applies to the four-section TCC unit, provided that m_1 and m_4 fulfill the relevant constraints, Eqs. 41 and 43.

Results and Discussion

Let us now investigate a few applications of the developed procedure that are not possible using the standard Triangle Theory. First, the complete separation region is determined for systems characterized by the binary bi-Langmuir isotherm. Second, the general validity of the developed procedure is shown with reference to systems described by the general multicomponent equilibrium model based on the Ideal Adsorbed Solution (IAS) Theory; in particular, the case where single-component Langmuir isotherms are combined according to the IAS theory to describe the competitive adsorption of a binary mixture is presented and discussed. It is worth noting that in both cases, that is, bi-Langmuir and IAS, only systems fulfilling the constraints given by Eqs. 15 to 20 in the preceding section, and Eqs. B1 to B3 in Appendix B can be considered. Finally, a shortcut method to determine an approximate region of complete separation is introduced and compared with the results of the rigorous approach previously presented.

Bi-Langmuir isotherm

Let us consider the binary bi-Langmuir isotherm:

$$n_i = \frac{\gamma_i c_i}{1 + \sum_{j=A,B} a_j c_j} + \frac{\delta_i c_i}{1 + \sum_{j=A,B} b_j c_j} \quad (i = A, B). \quad (44)$$

This favorable isotherm is well known in chromatography and is often used to describe adsorption on two independent sites, which is the case of a number of enantioseparations. The adsorbed amount in the stationary phase is given by the sum of two Langmuir terms. Usually one term accounts for the adsorption on nonchiral selective sites with high saturation capacity, while the other accounts for adsorption on chiral sites with low saturation capacity (Charton et al., 1993; Fornstedt et al., 1997). In many cases of applicative interest, the nonconstant selectivity behavior exibited by enantiomers on chiral stationary phases is properly described by this model. The bi-Langmuir isotherm can also be used as an empirical model to describe systems with selectivity strongly changing with composition, since it provides four parameters for each component to fit the equilibrium data.

Note that the Langmuir model can be obtained as a special case of the bi-Langmuir isotherm by letting $b_i = \delta_i = 0$ in Eq. 44, and the modified Langmuir model by letting $\delta_i = h$ and $b_i = 0$. The linear case, which is obtained by letting $a_i = b_i = 0$, is of particular interest because it represents the limit behavior of Eq. 44 in the case of very dilute solutions. It is seen that in all these cases the results already published in the literature are in agreement with the approach presented in this article.

Let us consider the separation of the enantiomers of 1-1′-bi-2-naphthol on a 3,5-dinitrobenzoyl phenylglycine bonded to silica gel stationary phase, using a mixture of heptane-hexane (78:22) as the mobile phase (Pais et al., 1997). The corresponding complete separation region calculated using the method discussed earlier is shown in Figure 7; the bi-Langmuir isotherm parameters are reported in the caption of Figure 6, and the feed concentration adopted for both enantiomers is $c_A^F = c_B^F = 2.9$ g/L. The region has a triangular shape where, contrary to the Langmuir case, the boundary *wb*, whose equation can still be written in a closed form since c_A^2 can be explicitly obtained from Eq. 32, is a curve and not a straight line (Gentilini et al., 1998). The complete separation region is surrounded by three more regions, corresponding to different separation regimes: pure extract, pure raffinate, and no pure outlet, that is, both components distributed in both outlet streams. Based on the graphical representation reported in Figure 7, from the relative position of the operating point with respect to the four regions, the SMB separation performance can be predicted, provided that the constraints discussed in the subsection on the four-section TCC unit, on the regenerating sections are fulfilled (Migliorini et al., 1999a). It is worth recalling that point *w* represents the optimal operating point in terms of process performance (Storti et al., 1993).

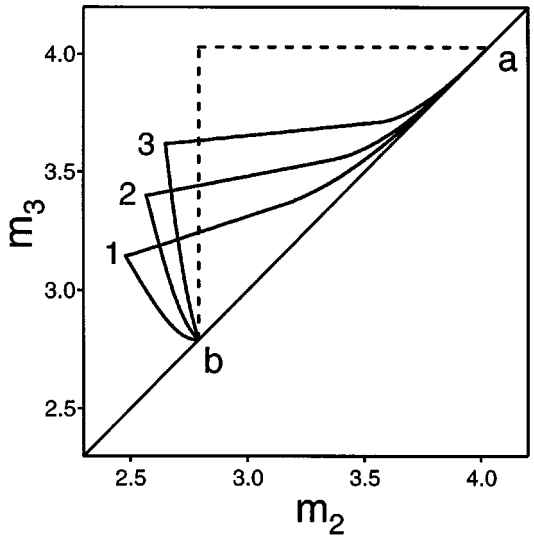

Figure 8. Effect of the total feed concentration on the region of complete separation in the (m_2, m_3) plane for a system described by a bi-Langmuir adsorption isotherm.

Isotherm parameters as in Figure 6: $c_A^F = c_B^F = c_T^F/2$. (1) $c_T^F =$ 5.8 g/L; (2) $c_T^F = 3$ g/L; (3) $c_T^F = 1.4$ g/L; (– – –) region of separation in the linear case, that is, when $c_T^F \to 0$.

The developed model is rather useful for gaining insight about the effect of feed composition on the SMB behavior, which is one of the main operating variables in industrial applications; this is done in Figures 8 and 9. In the former, the same separation with the same feed ratio of the components to be separated but different values of the overall feed concentration is considered. In the latter, the overall feed concentration is constant, that is, $c_T^F = c_A^F + c_B^F = 5.8$ g/L, but the relative composition of the two components in the feed changes. Figure 8 illustrates that when the overall feed concentration increases from infinite dilution (corresponding to the dashed right triangle) to larger values, the complete separation region becomes smaller and sharper (Mazzotti et al., 1996b). The optimal point shifts toward the lower left corner of the (m_2, m_3) plane, and the best feed concentration has to be chosen as a compromise between process performance, which improves for larger values of c_T^F, and robustness, which becomes smaller instead, as in the case of Langmuir isotherms (Mazzotti et al., 1997a). The effect of changing feed composition at constant overall feed concentration is quantitatively different and qualitatively less important than changing the overall feed concentration, as illustrated in Figure 9.

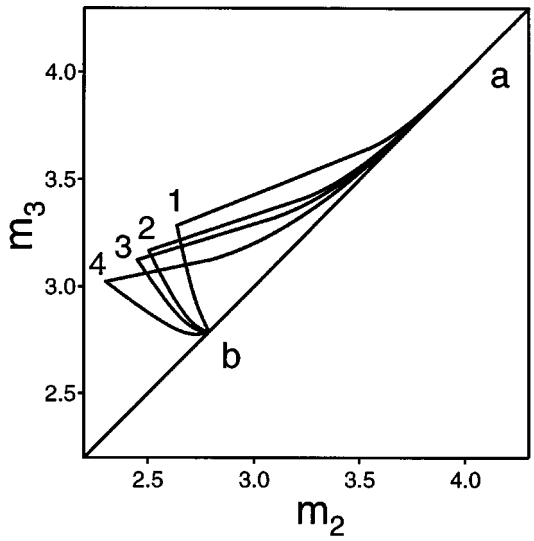

Figure 9. Effect of the relative feed composition on the region of complete separation in the (m_2, m_3) plane for a system described by a bi-Langmuir adsorption isotherm.

Isotherm parameters as in Figure 6: $c_T^F = 5.8$ g/L. (1) $c_A^F/c_T^F = 0.2$; (2) $c_A^F/c_T^F = 0.4$; (3) $c_A^F/c_T^F = 0.6$; (4) $c_A^F/c_T^F = 0.8$.

IAS model

A rather powerful tool for the description of complex adsorption equilibria where selectivity is a strong function of composition and adsorbate–adsorbate interaction are observed is provided by the Real Adsorbed Solution Theory (Gamba et al., 1989). Although the developed approach also can be applied to this model, for the sake of simplicity we limit ourselves to the IAS Theory model in the case where the pure-component isotherms are Langmuir (LeVan and Vermeulen, 1981). It is worth noting that Eqs. 15 to 20 in the section on design and operating conditions and Eqs. B1 to B3 in Appendix B are such that, on the one hand, not all systems described by single-component Langmuir isotherms and the IAS model fulfill them (cf. for instance, the systems with selectivity reversal described by Antia and Horváth, 1991). On the other hand, other IAS binary systems also fulfill the constraints, even though the single-component isotherms are not Langmuir.

The following set of ten equations in the ten unknowns, n_i, z_i, c_i^0, n_i^0, n, and Ψ ($i = A, B$), which can be solved in terms of c_A and c_B, describe the adsorption equilibrium:

$$c_i = z_i c_i^0 \qquad (i = A, B) \qquad (45)$$

$$\Psi = \int_0^{c_i^0} \frac{n_i^0(x)}{x}\,dx = N_i \ln\left(1 + K_i c_i^0\right) \qquad (i = A, B) \qquad (46)$$

$$1 = z_A + z_B \qquad (47)$$

$$n_i^0 = \frac{N_i K_i c_i^0}{1 + K_i c_i^0} \qquad (i = A, B) \qquad (48)$$

$$n_t = \left(\frac{z_A}{n_A^0} + \frac{z_B}{n_B^0}\right)^{-1} \qquad (49)$$

$$n_i = n_t z_i \qquad (i = A, B). \qquad (50)$$

Here Ψ represents the excess surface potential, which is proportional to the spreading pressure in the case of surface adsorption. An interesting situation arises in the case where the pure components exhibit different saturation concentrations, that is, $N_A \neq N_B$ in the corresponding Langmuir isotherm. In this case the IAS model fulfills the Gibbs adsorption isotherm (Eq. 46) and accounts for the effect of composition on selectivity. On the contrary the empirical constant selectivity mul-

ticomponent Langmuir model based on the same pure-component isotherms,

$$n_i = \frac{N_i K_i c_i}{1 + K_A c_A + K_B c_B} \qquad (i = A, B), \qquad (51)$$

is thermodynamically inconsistent. The two models coincide only when $N_A = N_B$. It should be emphasized that the IAS model is considered to be the correct one for ideal solutions, the binary Langmuir model being just its empirical approximation.

Let us now compare the complete separation region obtained with the multicomponent Langmuir isotherm, given by known explicit relationships in terms of the feed composition (Mazzotti et al., 1997a), and those obtained using the IAS model for which the developed procedure has to be applied. It is also worth noting that, while in the first case selectivity is constant, in the second one it changes with composition. Four cases are considered as reported in Table 2 in all of which the Henry constants of A and B, that is, $H_i = N_i K_i$, have been kept constant, but the ratio N_A/N_B has been changed, taking the values 4, 2, 0.5, and 0.25. The case where $N_A/N_B = 1$ is trivial, because in this case the two models coincide. The behavior of selectivity, defined as

$$S = \frac{n_A/n_B}{c_A/c_B}, \qquad (52)$$

as a function of the concentration of A or B for an equimolar mixture, is illustrated in Figure 10. It can be seen that according to the multicomponent Langmuir model $S = 2$ in all cases at all fluid concentrations, while in the case of the IAS model, selectivity increases or decreases for increasing values of c_A and c_B, depending on whether the ratio N_A/N_B is larger or smaller than one, respectively.

In Figures 11a–11d the complete separation regions, calculated with the binary Langmuir isotherm and with the IAS model, are compared. It appears that in all four cases the IAS prediction is rather different from the complete separation region obtained with the binary Langmuir isotherm. This difference is larger, the larger the difference between N_A and N_B (cf. the systems depicted in Figures 11a and 11d). In particular, the error made using the Langmuir isotherm in predicting the optimal operating point under the assumptions of Equilibrium Theory, that is, the vertex of the triangle, is rather large for the systems in Figures 11a and 11d. Moreover, the IAS "triangle" is smaller when $N_A < N_B$ and larger when $N_A > N_B$ than the region calculated with the binary Langmuir

Table 2. Single-Component Langmuir Isotherms Used for the Calculations in Figures 10 and 11

System	N_A	N_B	K_A	K_B	c_T^F
a	4	1	1	2	0.30
b	3	1.5	1.33	1.33	0.34
c	1.5	3	2.67	0.67	0.27
d	1	4	4	0.5	0.20

Note: The total feed concentrations c_T^F and the saturation capacities N are in g/L, the K values in L/g. The feed composition is equimolar.

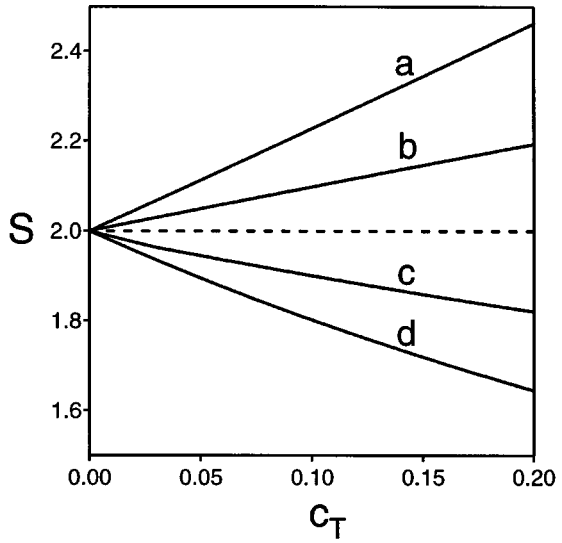

Figure 10. IAS model (solid lines) vs. multicomponent Langmuir isotherm (broken line).

Selectivity as a function of the total fluid concentration c_T for an equimolar mixture. The parameters for cases $a-d$ are reported in Table 2.

isotherm. The l.h.s. boundary of the complete separation region—line *wb*—is curved, and it is convex in the former case and concave in the latter. Finally, the tail of the complete separation region for high values of m_2 that is, the portion *ra* of the boundary coincides using the two models. This is consistent with the fact that Eq. 33, which is used to calculate *ra*, depends only on the pure-component A isotherm, which is the same for the two models.

This regular pattern of behavior can be explained by analyzing how selectivity changes with composition, as illustrated in Figure 10. Let us refer to the system in Figure 11a: in this case, the selectivity exhibited by the IAS model increases with respect to the constant Langmuir value when the concentration of the fluid increases. The average concentration in the TCC unit, as well as in the equivalent SMB, is larger for larger values of the difference $(m_3 - m_2)$, that is, for operating points far from the diagonal. It follows that when the IAS model is used, the TCC unit experiences selectivity values larger than when the binary Langmuir model is adopted; hence the complete separation region predicted using the former model is larger than the one calculated with the latter, thus indicating an easier and potentially more efficient separation. As a consequence, choosing the Langmuir model instead of the IAS model would lead to a wrong choice of the optimal operating point. The differences between the two regions are small in the zone close to the diagonal, since the difference in selectivities for the two models also is small for the small concentrations considered here, that is, with a relatively small feed flow rate. However, these differences are rather significant at larger feed concentration, that is, in the region where it is attractive from the application viewpoint to operate a TCC or an SMB unit. Similar observations can be repeated to explain the results obtained for the systems in Figures 11b, 11c and 11d. In particular, if the selectivity predicted by the IAS model is smaller than that given by the

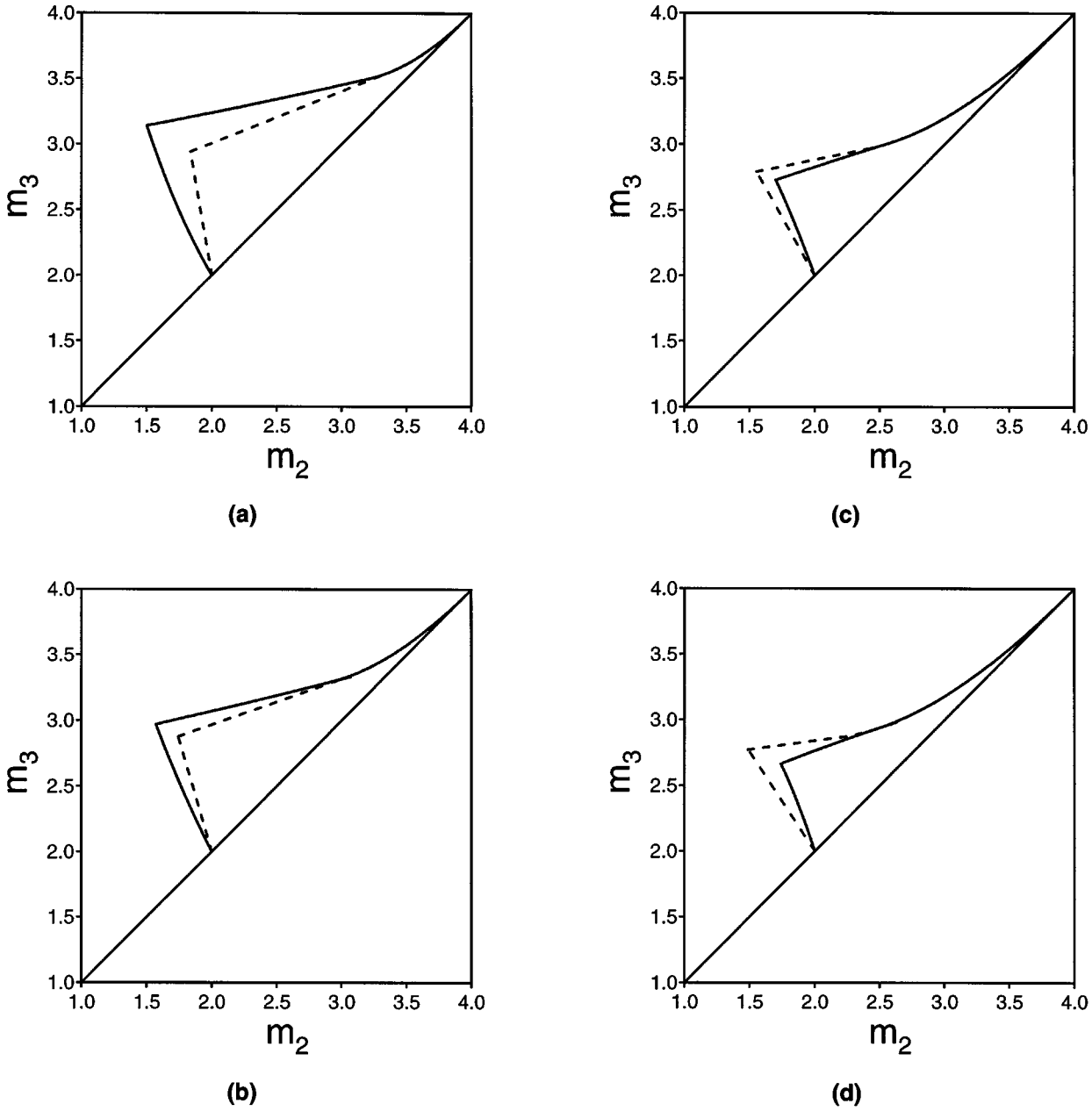

Figure 11. IAS model (solid lines) vs. multicomponent Langmuir isotherm (broken lines).

Regions of complete separation in the (m_2, m_3) plane for the different systems of Table 2.

binary Langmuir model, as in the case of the systems in Figures 11c and 11d, then the IAS complete separation region shrinks with respect to the Langmuir one.

Shortcut method

In this section we develop a shortcut method that allows, with a much simpler mathematical procedure, a good approximation of the complete separation region given by the general procedure developed earlier to be estimated. This appears particularly reasonable when considering that the Equilibrium Theory approach is in any case approximate, and therefore adding further approximation may be to a certain extent acceptable. The Equilibrium Theory model is in fact based on a simplified description of the adsorption column dynamics where mass transfer resistance and axial mixing are neglected. The effect of these dispersive phenomena on SMB performance can be accounted for using detailed models, as discussed by Migliorini et al. (1999a). In practice, dispersive phenomena shrink the complete separation region obtained through Equilibrium Theory. On the other hand, the adsorption equilibrium model adopted to describe the system of interest inevitably contains some approximations due to our limited understanding of adsorption on complex stationary phases, such as the ones used in chiral separations. In all cases, as we will see later, the errors introduced by the short-

cut method are of the same order of magnitude as the inherent inaccuracies of the Equilibrium Theory described earlier. The most valuable information given by the Triangle Theory refers to the position of the optimal operating point in the operating parameter space as a function of feed composition, as illustrated in Figures 8 and 9 in the case of the bi-Langmuir isotherm. This information allows the practitioner to choose a reasonable feed composition as a compromise between productivity and process robustness, to give a prediction of the process performance, and to effectively initialize a process optimizer that uses a detailed model of the TCC or SMB unit. It is worth pointing out that the effect of changing the feed composition on the shape and position of the complete separation region is indeed the key advantage provided by Triangle Theory. In fact, although a rough location of the optimal operating point is obtained through knowing the Henry's constants of the components to be separated, that is, assuming linear conditions for the separation, this is clearly a rather unsatisfactory approximation in most cases (Mazzotti et al., 1997a; Migliorini et al., 1998).

This information can be achieved through the following simplified procedure, where it is assumed that a competitive binary isotherm for the system under examination is available. In other words, the relationships shown in Eqs. 18 and 19 are known and the conditions of Eqs. 15 to 20 are fulfilled. It is further assumed that the conditions discussed in Appendix B are fulfilled, even though there is no way to check them when applying the shortcut method.

With reference to Figure 7, for example, curves *wb* and *ra* of the boundary of the complete separation region are calculated using the procedure described in the subsection on the complete separation region. In fact Eqs. 32 and 33 are simple enough to be handled in the most general case, and in the important case of bi-Langmuir isotherm and IAS model, explicit relationships for lines *wb* and *ra* can be easily obtained.

The most difficult step of the general procedure is the calculation of curve *wr*, which reflects the strong coupling between the two central sections of the TCC unit. The shortcut method consists of substituting the correct curve *arw* with the approximate line *aw′*, which is given by the following two relationships, obtained by combining Eqs. 35, 38, and 40:

$$m_3 = \frac{n_A^\beta}{c_A^\beta} \tag{53}$$

$$m_2 = m_3 + \frac{n_B^\beta - m_3 c_B^\beta}{c_B^F}. \tag{54}$$

If these equations were applied using the composition of state $\boldsymbol{\beta}$ properly coupled to the feed state and to states $\boldsymbol{\alpha}$ and $\boldsymbol{\gamma}$ (see Figure 6), then the correct curve *rw* would be obtained. However, one can see that point $\boldsymbol{\beta}$ in the hodograph plane is confined in the region between the origin and the feed state. Thus, as a first approximation it can be assumed that the state $\boldsymbol{\beta}$ is located on the straight line $D \rightarrow F$. This implies choosing values of c_A^β between zero and c_A^F, and accordingly $c_B^\beta = c_A^\beta c_B^F / c_A^F$. Entering this set of values into Eqs. 53 and 54 leads directly to the coordinates of the points on the line *a w′a′* in Figure 12a. It is worth noting that when $c_A^B = 0$, the preceding equations yield the coordinates of point

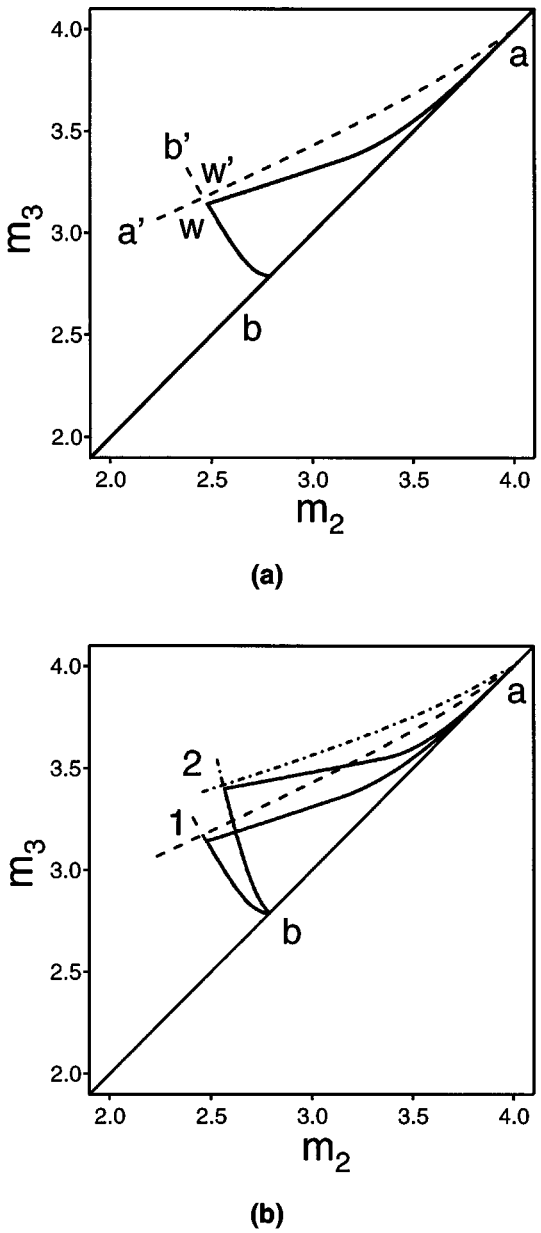

Figure 12. Regions of complete separation calculated with the rigorous procedure (solid lines) and with the shortcut method (broken lines) for a bi-Langmuir isotherm (see Figure 6 for the parameters).

$c_A^F = c_B^F = c_T^F = c_T^F/2$. (a) $c_T^F = 5.9$ g/L. The optimal operating point *w′* calculated with the shortcut approach is close to the point *w*. (b) Effect of feed concentration: (1) $c_T^F = 5.8$ g/L, (2) $c_T^F = 3$ g/L. The effect of the feed concentration is well accounted for by the shortcut solution.

a, that is, (H_A, H_A). This is why this curve is also taken as an approximation of line *ra*, which is replaced by it.

Based on these observations, the shortcut algorithm reported in Table 3 and illustrated in Figure 12a is proposed. The shortcut complete separation regions for the same system used to draw Figures 8 and 9 and for the overall feed concentrations 3 and 5.8 g/L are compared in Figure 12b, with the exact solution. It can be readily observed that not

Table 3. Shortcut Calculation Procedure of the Approximate Complete Separation Region in the (m_2, m_3) Plane

Curve bwb′		
Step 1	take c_A^2 in the range $0 \le c_A^2 \le c_A^F$	
Step 2	$m_2 = \partial n_B/\partial c_B\vert_{(c_A^2, 0)}$	—see Eqs. 19 and 32
Step 3	$m_3 = m_2 + (n_A^2 - m_2 c_A^2)/c_A^F$	—see Eqs. 18 and 39
Curve aw′a′		
Step 4	take c_A^β in the range $0 \le c_A^\beta \le c_A^F$	
Step 5	$c_B^\beta = c_A^\beta c_B^F/c_A^F$	
Step 6	$m_3 = n_A^\beta/c_A^\beta$	—see Eqs. 18 and 53
Step 7	$m_2 = m_3 + (n_B^\beta - m_3 c_B^\beta)/c_B^F$	—see Eqs. 19 and 54
Point w′		
Step 8	take point w' as the intersection between curves bwb' and $aw'a'$	

only is the shortcut method able to reproduce qualitatively the effect of changing feed concentration on the shape of the complete separation region but it is also remarkably accurate in predicting the position of the optimal operating point. It is worth noting that the accuracy of the shortcut method is not very good at rather small values of $(m_3 - m_2)$, which in any case are not very attractive in practice, since they correspond to low productivity. It should be remarked that lines $w'b'$ and $w'a'$ have no physical meaning, since they have been obtained by enforcing the overall material balances of Eqs. 39 and 40, which hold true only under complete separation conditions.

This analysis proves that the shortcut method may be a rather effective tool for determining approximate complete separation regions for two kinds of systems: those described by complex isotherms for which the exact procedure reported in the subsection titled ''The Complete Separation Region'' is not doable and those described by isotherms such as bi-Langmuir or IAS for which the exact procedure is feasible, but does not lead to close algebraic expressions as in the Langmuir case. Whenever an algebraic first approximation of the exact region of complete separation is required, the shortcut algorithm in Table 3 provides very fast and rather accurate information. The key drawback of this method is that it does not allow one to check the prerequisites for the application of the theory presented in this work and discussed in Appendix B. For this, one has to rely on physical intuition.

Concluding Remarks

This work provides a new tool that allows the Equilibrium Theory approach for the design of binary countercurrent adsorptive separation units to be extended to a larger class of isotherms. This conclusion is particularly important in view of the wider and wider application of continuous chromatography, through the SMB technology, in the chemical and pharmaceutical industries. Using as examples the bi-Langmuir isotherm and the IAS model, a general mathematical procedure is illustrated that also can be applied to other isotherms. Some calculations show how the procedure described earlier can be used to analyze in a rather straightforward way important aspects of the continuous chromatography technology, including the effect of feed composition. Finally, a simplified procedure that allows the mathematical complexity of the involved calculations to be reduced, leading only to explicit algebraic relations, without significantly affecting the accuracy of the final results, is discussed.

Notation

a_i = adsorption equilibrium constant in bi-Langmuir isotherms
b_i = adsorption equilibrium constant in bi-Langmuir isotherms
c_i = fluid-phase concentration of species i
D = pure eluent state
h = constant linear term in the modified Langmuir model
H_i = Henry constant of species i
M_j = intermediate state of sections 2 and 3
N = saturation capacity in the Langmuir model defined by Eq. 48
n_i = adsorbed-phase concentration of species i
Q = volumetric flow rate
t^* = switch time in a SMB unit
V = volume of the column
x = dimensionless column coordinate, $x = z/L$
z = column coordinate
$\boldsymbol{\alpha}$ = fluid state leaving section 2 in TCC unit
β_k = substantial derivative along a Γ Transition
γ_i = adsorption equilibrium constant in bi-Langmuir isotherms for species i
Γ = simple wave locus in the hodograph plane
$\boldsymbol{\delta}$ = fluid state entering section 2 in the 4-section TCC unit
δ_i = adsorption equilibrium constant in bi-Langmuir isotherms for species i
$\boldsymbol{\epsilon}$ = solid state entering section 3 in the 4-section TCC unit
ϵ^* = overall void fraction of the bed, defined as $\epsilon^* = \epsilon_b + (1 - \epsilon_b)\epsilon_p$
ϵ_b = bed or interparticle void fraction
ϵ_p = intraparticle void fraction
λ = speed of characteristic of a simple wave in the (τ, x) plane
σ = slope of characteristic of a simple wave in the (τ, x) plane
Σ = shock locus in the hodograph plane
τ = dimensionless time, tQ_S/V
ζ = local slope of a Γ locus in the hodograph plane, defined by Eq. (A3)
ϕ = fluid state leaving section 3 in 2-section TCC unit
ψ = solid state leaving section 2 in 2-section TCC unit
Ψ = excess surface potential defined by Eq. 46

Subscripts and superscripts

E = extract
F = feed
i = component index, $i = A, B$
j = section index, $j = 1, \ldots, 4$
k = transition range, $k = 1, 2$
R = raffinate
S = solid
0 = single-component isotherm

Literature Cited

Antia, F. D., and C. Horváth, ''Analysis of Isotachtic Patterns in Displacement Chromatography,'' *J. Chromatog.*, **556**, 119 (1991).

Charton, F., S. C. Jacobson, and G. Guiochon, ''Modeling of the Adsorption Behavior and the Chromatographic Band Profile of Enantiomers,'' *J. Chromatog. A*, **630**, 21 (1993).

Chiang, A. S. T., ''Complete Separation Conditions for a Local Equilibrium TCC Adsorption Unit,'' *AIChE J.*, **44**, 332 (1998a).

Chiang, A. S. T., ''Equilibrium Theory for Simulated Moving Bed Adsorption Processes,'' *AIChE J.*, **44**, 2431 (1998b).

Fornstedt, T., P. Sjonz, and G. Guiochon, ''Thermodynamic Study of an Unusual Chiral Separation: Propanol Enantiomers on an Immobilised Cellulase,'' *J. Amer. Chem. Soc.*, **119**, 1254 (1997).

Francotte, E., J. Richert, M. Mazzotti, and M. Morbidelli, ''Simulated Moving Bed Chromatographic Resolution of Racemic Guaifenesin,'' *J. Chromatog. A*, **796**, 239 (1998).

Gamba, G., R. Rota, G. Storti, S. Carra, and M. Morbidelli, ''Adsorbed Solution Theory Models for Multicomponent Adsorption Equilibria,'' *AIChE J.*, **35**, 959 (1989).

Gentilini, A., C. Migliorini, M. Mazzotti, and M. Morbidelli, ''Optimal Operation of Simulated Moving Bed Units for Non-Linear Chromatographic Separations. II Bi-Langmuir Isotherms,'' *J. Chromatog. A*, **805**, 37 (1998).

Helfferich, H., and R. Klein, *Multicomponent Chromatography*, Dekker, New York (1970).

Jacobson, S., S. Golshan-Shirazi, and G. Guiochon, "Chromatographic Band Profile and Band Separation of Enantiomers at High Concentration," *J. Amer. Chem. Soc.*, **112**, 6492 (1990).
LeVan, M. D., and T. Vermeulen, "Binary Langmuir and Freundlich Isotherms for Ideal Adsorbed Solutions," *J. Phys. Chem.*, **85**, 3247 (1981).
Mazzotti, M., G. Storti, and M. Morbidelli, "Robust Design of Binary Countercurrent Separation Processes 2. Multicomponent Systems," *AIChE J.*, **40**, 1825 (1994).
Mazzotti, M., R. Baciocchi, G. Storti, and M. Morbidelli, "Vapor-Phase Simulated Moving Bed Adsorptive Separation of Linear/Nonlinear Paraffins," *Ind. Eng. Chem. Res.*, **35**, 2313 (1996a).
Mazzotti, M., G. Storti, and M. Morbidelli, "Robust Design of Binary Countercurrent Separation Processes 3. Nonstoichiometric Systems," *AIChE J.*, **42**, 2784 (1996b).
Mazzotti, M., G. Storti, and M. Morbidelli, "Optimal Operation of Simulated Moving Bed Units for Nonlinear Chromatographic Separations," *J. Chromatog. A*, **769**, 3 (1997a).
Mazzotti, M., G. Storti, and M. Morbidelli, "Robust Design of Binary Countercurrent Separation Processes 4. Desorbent in the Feed," *AIChE J.*, **43**, 64 (1997b).
Migliorini, C., M. Mazzotti, and M. Morbidelli, "Continuous Chromatographic Separation Through Simulated Moving Beds Under Linear and Nonlinear Conditions," *J. Chromatog. A*, **827**, 161 (1998).
Migliorini, C., A. Gentilini, M. Mazzotti, and M. Morbidelli, "Design of Simulated Moving Bed Units Under Non-Ideal Conditions," *Ind. Eng. Chem. Res.*, **38**, 2400 (1999a).
Migliorini, C., M. Mazzotti, and M. Morbidelli, "Simulated Moving Bed Units with Extracolumn Dead Volume," *AIChE J.*, **45**, 1411 (1999b).
Pais, L. S., J. M. Loureiro, and A. E. Rodrigues, "Modeling, Simulation and Operation of a Simulated Moving Bed for Continuous Chromatographic Separation of 1-1′-bi-2-Naphtol Enantiomers," *J. Chromatog. A*, **769**, 25 (1997).
Pedeferri, M., G. Zenoni, M. Mazzotti, and M. Morbidelli, "Experimental Analysis of a Chiral Separation Through Simulated Moving Bed Chromatography," *Chem. Eng. Sci.*, **54**, 3735 (1999).
Radke, C. J., and J. M. Prausnitz, "Thermodynamics of Multi-Solute Adsorption from Dilute Liquid Solutions," *AIChE J.*, **18**, 761 (1972).
Rhee, H.-K., R. Aris, and N. R. Amundson, "On the Theory of Multicomponent Chromatography," *Phil. Trans. R. Soc. London*, **A267**, 419 (1970).
Rhee, H.-K., R. Aris, and N. R. Amundson, *First Order Partial Differential Equations*, Vol. I, Prentice Hall, Englewood Cliffs, NJ (1986).
Rhee, H.-K., R. Aris, and N. R. Amundson, *First Order Partial Differential Equations*, Vol. II, Prentice Hall, Englewood Cliffs, NJ (1989).
Ruthven, D. M., and C. B. Ching, "Counter Current and Simulated Counter Current Adsorption Separation Processes," *Chem. Eng. Sci.*, **44**, 1011 (1989).
Seidel-Morgenstern, A., and G. Guiochon, "Modeling of the Competitive Isotherms and the Chromatographic Separation of Two Enantiomers," *Chem. Eng. Sci.*, **48**, 2787 (1993).
Storti, G., M. Mazzotti, M. Morbidelli, and S. Carrá, "Robust Design of Binary Countercurrent Separation Processes," *AIChE J.*, **39**, 471 (1993).

Appendix A

The mass-balance equations of the single countercurrent chromatographic column (Eq. 3) can be solved using the method of characteristics (Rhee et al., 1989). Along the characteristics in the physical plane (x,τ), the balance equations are equivalent to the following fundamental equations (written here in the case of a binary system):

$$\left.\frac{Dn_A}{Dc_A}\right|_{\Gamma_k} = \left.\frac{Dn_B}{Dc_B}\right|_{\Gamma_k} = \beta_k \qquad (k=1,2). \tag{A1}$$

The parameters β_k are the eigenvalues of the matrix $\nabla n = [\partial n_i/\partial c_j]$. For a binary system, these eigenvalues can be calculated as follows:

$$\frac{\partial n_B}{\partial c_B} + \frac{\partial n_B}{\partial c_A}\zeta_k = \frac{\partial n_A}{\partial c_A} + \frac{1}{\zeta_k}\frac{\partial n_A}{\partial c_B} = \beta_k, \tag{A2}$$

where the value of ζ is given by

$$\zeta = \frac{dc_A}{dc_B} = \frac{1}{2}\left(\frac{\partial n_B}{\partial c_A}\right)^{-1}\left[\left(\frac{\partial n_A}{\partial c_A} - \frac{\partial n_B}{\partial c_B}\right) \pm \sqrt{\left(\frac{\partial n_A}{\partial c_A} - \frac{\partial n_B}{\partial c_B}\right)^2 + 4\frac{\partial n_A}{\partial c_B}\frac{\partial n_B}{\partial c_A}}\right] \tag{A3}$$

It is worth recalling that ζ_1 and ζ_2 are calculated from the last equation using the minus and plus sign, respectively, hence due to Eqs. 15, $\zeta_1 > 0 > \zeta_2$.

Using Eq. A1, the slope of the characteristics in the physical plane is given by

$$\sigma_k = \frac{\epsilon^* + (1-\epsilon^*)\beta_k}{(1-\epsilon_p)(m-\beta_k)} \qquad (k=1,2), \tag{A4}$$

and the corresponding characteristic speed by

$$\lambda_k = \frac{1}{\sigma_k} = \frac{(1-\epsilon_p)(m-\beta_k)}{\epsilon^* + (1-\epsilon^*)\beta_k} \qquad (k=1,2). \tag{A5}$$

Equation A1 defines two families of characteristics, Γ_1 and Γ_2, in the hodograph plane, spanned by the fluid-phase concentrations (c_A, c_B). These can be calculated by integrating the ordinary differential equation (Eq. A3). It is worth noting that in the neighborhood of the origin of the hodograph plane, the c_A and c_B axes are Γ_2 and Γ_1 characteristics, respectively.

By considering Eqs. A1, A2, and A3, it easily can be shown that $\beta_2 > \beta_1 > 0$; hence, due to Eq. A5, $\lambda_1 > \lambda_2$ whatever the value of m is.

From any starting point (c_A, c_B) in the hodograph plane, two loci, Σ_1 and Σ_2, emanate, each constituted of points reachable from the starting point through a shock transition, that is, fulfilling the generalized Rankine-Hugoniot relations, also called the jump conditions:

$$\tilde{\beta}_k = \left.\frac{[n_A]}{[c_A]}\right|_{\Sigma_k} = \left.\frac{[n_B]}{[c_B]}\right|_{\Sigma_k} \qquad (k=1,2), \tag{A6}$$

where $[\cdot]$ denotes the jump in the quantity enclosed across the discontinuity. A shock transition occurs in the chromatographic column whenever the characteristics of the simple wave transition tend to intersect, leading to infeasible solutions of the mass-balance equations. The corresponding propagation direction in the physical plane is given by:

$$\tilde{\sigma}_k = \frac{\epsilon^* + (1-\epsilon^*)\tilde{\beta}_k}{(1-\epsilon_p)(m-\tilde{\beta}_k)} \qquad (k=1,2), \tag{A7}$$

and the propagation speed by

$$\tilde{\lambda}_k = \frac{1}{\tilde{\sigma}_k} = \frac{(1-\epsilon_p)(m-\tilde{\beta}_k)}{\epsilon^* + (1-\epsilon^*)\tilde{\beta}_k} \qquad (k=1,2). \quad \text{(A8)}$$

In general Σ_k and Γ_k are different, with Σ_k having a third-order contact at (c_A, c_B), with Γ_k; in the special case of the Langmuir isotherm, where the characteristics are straight lines, Σ_k and Γ_k coincide for every point (c_A, c_B). In the case of a general isotherm, being the c_A and c_B axis Γ curves, they are at the same time Σ curves. Therefore if one of the feed states (fluid or stationary phase) entering the countercurrent section of Figure 3 is constituted of a pure component (or it is pure desorbent), then the point corresponding to the intermediate state lies on one of the axes.

Appendix B

It is worth noting that c_A and c_B change in the same direction along a Σ_1 or a Γ_1, that is, both A and B either increase or decrease, whereas along a Σ_2 or a Γ_2 they change in the opposite direction. Along a path on a given characteristic, Γ_k, the characteristic speed, λ_k, may increase or decrease or even first increase and then decrease; these different behaviors yield continuous simple wave transitions, discontinuous shock waves, or combined waves, respectively, when this path is mapped onto the physical plane (Rhee et al., 1989). In the case of a general adsorption isotherm, different situations can be observed in different regions of the hodograph plane.

However, in this work we restrict our analysis to those isotherms that exhibit the following behavior:

- Along a characteristic Γ_1 the characteristic speed increases in the direction of increasing values of both c_A and c_B; this can be expressed in mathematical form as

$$\left.\frac{\partial \lambda_1}{\partial c_A}\right|_{\Gamma_1} > 0; \quad \text{(B1)}$$

- Along a characteristic Γ_2 the characteristic speed increases in the direction of increasing values of c_A, that is, of decreasing values of c_B; this can be expressed in mathematical form as

$$\left.\frac{\partial \lambda_2}{\partial c_A}\right|_{\Gamma_2} > 0. \quad \text{(B2)}$$

Since for a two-section TCC unit the transition Γ_2 occurs along the c_A axis (see Figure 5) and involves a single component, it is possible to prove that the constraint represented by Eq. B2 is always fulfilled when the conditions introduced in the section on the design and operating conditions—Eqs. 15 to 20—hold true.

The assumptions just reported guarantee that the transitions in the section on the design problem of the TCC unit are waves (see Figure 5). The condition given by Eq. B1 can be verified while integrating along Γ_1, to determine the curve *wr*, as discussed in the subsection on the two-section TCC unit.

Let us now consider the conditions that guarantee that the transition of the TCC unit in the section on the design of the operating condition are shocks. It is easy to prove that the single-component transition Σ_1, which lies on the c_B axis, is a shock provided that Eq. 20 is fulfilled. On the contrary, the stability conditions for the shock transitions Σ_2 in Figure 5, which involves both components, are more complex. In fact, Eq. B2 tells us that starting from point $\boldsymbol{\beta}$ in the hodograph plane a Γ_2 transition is not feasible, because characteristics would intersect. Moreover, the stability of the shock Σ_2 has to be checked pointwise along Σ_2 itself, so as to make sure that more complex transitions, such as semishocks, do not occur. This requires that for every point p along Σ_2 the following condition holds:

$$\tilde{\lambda}_2(c_A^\beta, c_B^\beta, c_A^p, c_B^p) > \lambda_2(c_A^p, c_B^p). \quad \text{(B3)}$$

Appendix C

Since a k-section TCC unit is the combination of k single countercurrent sections, the results summarized in Appendix A about the steady-state behavior of a single countercurrent column can be directly used here.

With reference to Figure 4, let us consider for the time being that states $\boldsymbol{\beta}$ and $\boldsymbol{\gamma}$ are generic and independent two-component states in the hodographic plane, as illustrated in Figure 5; this implies that their coupling through the mass balance at the bottom of section 3 is not yet accounted for. Note that for the sake of generality in the following we assume that the fluid stream entering section 2 may contain some of the more adsorbable component A; hence, its representative point in Figure 5 is point $\boldsymbol{\epsilon}$. Accordingly, the solid stream entering section 3 may contain some of the less retained component B, that is, its corresponding point in the hodograph plane is point $\boldsymbol{\delta}$. This allows the results presented shortly to be applied to both the two- and the four-section TCC unit.

From the results of Appendix A and of the subsection on the two-section TCC unit the following conclusions can be readily drawn:

Section 2. The image of the solution in the hodograph plane is given by the path $\boldsymbol{\epsilon} \rightarrow M_2 \rightarrow \boldsymbol{\gamma}$, constituted of portions of a Γ_2 and a Γ_1 characteristic, that is, simple waves. The bounds defining the different ranges for the flow-rate ratio in section 2, m_2, are given by the following relationships:

$$m_1^* = \beta_1|_\gamma, \quad \text{(C1)}$$

$$m_{1,*} = \beta_1|_{M_2} = \left.\frac{\partial n_B}{\partial c_B}\right|_{(c_A^2, 0)}, \quad \text{(C2)}$$

$$m_2^* = \beta_2|_{M_2} = \left.\frac{\partial n_A}{\partial c_A}\right|_{(c_A^2, 0)}, \quad \text{(C3)}$$

$$m_{2,*} = \beta_2|_\epsilon = \left.\frac{\partial n_A}{\partial c_A}\right|_{(c_A^\epsilon, 0)}, \quad \text{(C4)}$$

where the superscripts 2 and ϵ refer to the states M_2 and $\boldsymbol{\epsilon}$, respectively, and $\beta_1|_{M_2}$ depends only on point M_2 through Eqs. A2 and A3.

Section 3. The image of the solution in the hodograph plane is given by the path $\boldsymbol{\beta} \rightarrow M_3 \rightarrow \boldsymbol{\delta}$, constituted of portions of a Σ_2 and a Σ_1 transition, that is, shock waves. The bounds defining the different ranges for the flow-rate ratio in section 3, m_3, are given by the following relationships:

$$m_1^* = m_{1,*} = \tilde{\beta}_1|_{M_3 \rightarrow \delta} = \frac{n_B^3 - n_B^\delta}{c_B^3 - c_B^\delta}, \tag{C5}$$

$$m_2^* = m_{2,*} = \tilde{\beta}_2|_{\beta \rightarrow M_3} = \frac{n_A^\beta}{c_A^\beta} = \frac{n_B^\beta - n_B^3}{c_B^\beta - c_B^3}, \tag{C6}$$

where the superscripts 3, β, and δ refer to the states M_3, $\boldsymbol{\beta}$, and $\boldsymbol{\delta}$, respectively. It is worth noting that the former state is uniquely determined by the last equation once the state $\boldsymbol{\beta}$ is known.

The next step is to determine for each section which steady state among the possible achievable ones is compatible with the complete separation requirement. First, let us consider section 3, where due to the occurrence of two shock transitions only three states can be selected as constant steady states, namely $\boldsymbol{\beta}$, M_3, and $\boldsymbol{\delta}$; this can be made through a proper choice of m_3 according to the rules in Table 1. In this case, it is straightforward to demonstrate that the intermediate state M_3 is the only one compatible with complete separation; in fact, when Eqs. C5 and C6 are substituted in the constraints of Table 1, it turns out that the sign conditions (Eqs. 9 and 13), on the pure-component fluxes are fulfilled only when m_3 is within the intermediate range. In fact, if m_3 is selected within the lower range, then $f_B^3 = 0$ due to Eq. 20, whereas if m_3 is chosen within the upper range, then $f_A^3 > 0$.

In the case of section 2 all five ranges of values of m_2 reported in Table 1 need to be accounted for. The analysis is performed in the following with reference to the relevant sign conditions on the pure component fluxes (Eqs. 8 and 12).

Lower Range. This range is not feasible, since the 1-transition range is not feasible (see below) and for continuity reasons, even smaller values of f_B^2 than in the 1-transition range (where they are negative) are supposed to be observed.

1-Transition Range. Let us call I the steady state on the path $M_2 \rightarrow \boldsymbol{\gamma}$ achieved, with m_2 selected in this range; therefore $m_2 = \beta_1^I$. Using Eqs. 15, A2 and A3, it can be shown that

$$\beta_1^I < \min\left[\frac{\partial n_A}{\partial c_A}, \frac{\partial n_B}{\partial c_B}\right],$$

where the derivatives are calculated in I. It follows that $\beta_1^I < \partial n_B/\partial c_B < n_B^I/c_B^I$, due to Eq. 20. Therefore, $f_B^2 < 0$, contrary to the requirement (Eq. 8), which proves that the 1-transition range is not feasible.

Intermediate Range. This range is feasible, since $m_2 < (\partial n_A/\partial c_A)_{(c_A^2, 0)} < n_A^2/c_A^2$ implies $f_A^2 < 0$; on the other hand, due to Eq. 20, $m_2 > (\partial n_B/\partial c_B)_{(c_A^2, 0)} > (\partial n_B/\partial c_B)_{(c_A^2, c_B^2)}$ implies $f_B^2 > 0$, as required by Eqs. 12.

2-Transition Range. Let us call I the steady state on the path $\boldsymbol{\epsilon} \rightarrow M_2$ achieved with m_2 selected in this range. Since $c_B = 0$ along the whole characteristic Γ_2, to which point I belongs, using Eqs. A2 and A3 yields $m_2 = \beta_2^I = (dn_A/dc_A)$, where the derivative is calculated in I. The last equation is a one-to-one mapping between m_2 and c_A^I; substituting this into the overall mass-balance equation of component A under the assumption of complete separation yields the following relationship:

$$f_A^2 = m_2 c_A^I - n_A^I = -(m_3 - m_2) c_A^F, \tag{C7}$$

which is the equation of a curve in the (m_2, m_3) plane. Even though operating points on this line are feasible to achieve complete separation, they will not be considered any further, since they constitute a one-dimensional locus that is not attainable in practical applications (cf. the more detailed discussion about Figure 17 in Storti et al. (1993).

Upper Range. Since the constant steady-state is $\boldsymbol{\epsilon}$, then the same Eq. C7 with $I = \boldsymbol{\epsilon}$ applies when $m_2 = \mu_2^* = dn_A/dc_A$ with the last derivative calculated in c_A^ϵ applies, together with the considerations following Eq. A7. The $m_2 = \mu_2^*$ case is not feasible, since in this case Eq. C7 and the complete separation requirement (Eq. 8) would not hold true.

Therefore the intermediate state M_2 is the only compatible one with complete separation.

Manuscript received June 14, 1999, and revision received Feb. 15, 2000.